J Nanopart Res (2016) 18:267
DOI 10.1007/s11051-016-3582-z

RESEARCH PAPER

Zero-valent iron particles embedded on the mesoporous silica–carbon for chromium (VI) removal from aqueous solution

Kun Xiong · Yuan Gao · Lin Zhou · Xianming Zhang

Received: 8 June 2016 / Accepted: 27 August 2016 / Published online: 1 September 2016
© Springer Science+Business Media Dordrecht 2016

Abstract Nanoscale zero-valent iron (nZVI) particles were embedded on the walls of mesoporous silica–carbon (MSC) under the conditions of high-temperature carbonization and reduction and used to remove chromium (VI) from aqueous solution. The structure and textural properties of nZVI–MSC were characterized by the powder X-ray diffraction, transmission electron microscopy and N_2 adsorption and desorption. The results show that nZVI–MSC has highly ordered mesoporous structure and large surface area, indistinguishable with that of MSC. Compared with the support MSC and iron particles supported on the activated carbon (nZVI/AC), nZVI–MSC exhibited much higher Cr(VI) removal efficiency with about 98 %. The removal process obeys a pseudo first-order model. Such excellent performance of nZVI–MSC could be ascribed to the large surface and iron particles embedded on the walls of the MSC, forming an intimate contact with the MSC. It is proposed that this feature might create certain micro-electrode on the interface of iron particles and MSC, which prevented the formation of metal oxide on the surface and provided fresh Fe surface for Cr(VI) removal.

Keywords Zero-valent iron · Mesoporous silica–carbon · Embedded · Chromium · Environment · Remediation

K. Xiong (✉) · Y. Gao · X. Zhang
Engineering Research Center for Waste Oil Recovery Technology and Equipment of Ministry of Education, Chongqing Key Laboratory of Catalysis & Environmental New Materials, Chongqing Technology and Business University, Chongqing 400067, China
e-mail: kunxiong312@gmail.com

L. Zhou
Chengdu Radio and TV University, Chengdu 610051, Sichuan, China

Introduction

Chromium (Cr) has been increasingly discharged into water environment because of the growth in industrial activities from tanning factories, paint and pigment production, metallurgy and metal electroplating (Owlad et al. 2009). It usually exists in two relatively stable valence states, i.e., in the form of Cr(III) and Cr(VI) species, the latter of which has a more adverse impact on living organisms due to the high aqueous solubility, toxicity and carcinogenicity (Zhitkovich 2005). The US Environmental Protection Agency has set a Maximum Contaminant Level for Cr at 0.1 ppm in drinking water (Selvi et al. 2001). It is thus necessary and significant to remove chromium from water bodies.

Some conventional technologies have been widely employed to remove Cr(VI) from the polluted water, such as chemical precipitation, extraction, ion

exchange, electrocoagulation, membrane separation, adsorption and reduction (Miretzky and Cirelli 2010; Jiang et al. 2013; Wu et al. 2012). Among these technologies, chemical reduction–precipitation has been proved to be a high efficient and potential method for cleanup of Cr(VI) from the polluted water (Wang et al. 2013). Nanoscale zero-valent iron (nZVI), as an effective reducing agent, possesses large removal capacity, fast kinetics and high reactivity for pollutions (Wang et al. 2009; Singh et al. 2011; Lv et al. 2011; Zhang et al. 2013). When nZVI is oxidized to iron ions, Cr(VI) is reduced to Cr(III) followed by the precipitation in the form of sparingly soluble Cr or mixed Fe/Cr (oxy) hydroxides (Liu et al. 2009). However, nZVI particles are easy to be aggregation and oxidization due to the high surface energy, magnetization and high reactivity with water and oxygen in the water bodies (Zheng et al. 2013), which result in decreasing the reactive activity and limiting the application of nZVI particles. Recently, some research efforts have been devoted to avoiding the formation of passive layer and aggregation by using the porous materials as the supports, such as multiwalled carbon nanotubes, metal oxides, soil, activated carbon and SBA-15 (Lv et al. 2011; Sheng et al. 2016; Choi et al. 2008; Saad et al. 2010; Shipley et al. 2011). Although the phenomenon of aggregation are obviously inhibited over the nZVI particles to a certain degree, the nZVI particles loaded on the surface of the supports are still prone to be oxidized and lost during the further reaction because of their weak interaction between the nZVI particles and the supports.

Based on the above considerations, herein we develop a controllable method to address both the aggregation and oxidation of nZVI particles by constructing nZVI particles embedded on the walls of the mesoporous silica–carbon (MSC). Such feature might create certain micro-electrode on the interface of iron particles and the carbon of MSC, which prevented the formation of metal oxide on the surface and provided fresh Fe surface for Cr(VI) removal. The nZVI–MSC was characterized using X-ray diffraction (XRD), N_2 adsorption–desorption, and transmission electron microscopy (TEM). We also evaluated the removal efficiency, influence factors and the kinetics model fitting with Cr(VI) removal by nZVI–MSC.

Materials and methods

Materials

Analytical-grade tetraethylorthosilicate (TEOS), sucrose, ferric chloride hexahydrate and other agents were purchased from the Sinopharm Group Chemical Reagent, China. Triblock polymer Pluronic P123 ($EO_{20}PO_{70}EO_{20}$, $M_{AV} = 5800$) was obtained from Aldrich, USA. The stock standard solutions (1.0 g L^{-1}) of Cr(VI) were prepared by dissolving appropriate amounts of potassium chromate in ultrapure water.

Preparation of nZVI–MSC

MSC was synthesized as follows: 10.0 g of P123 and 8.0 g sucrose were stirred with 350 mL of 2 M HCl solution at 35 °C until completely dissolved. Subsequently, 22.5 g of TEOS was gradually added into the above solution. The mixture was continually stirred at 35 °C for 24 h, followed by hydrothermal treatment at 100 °C for 24 h in a polytetrafluoroethylene bottle. The precipitate was thoroughly washed with deionized water and dried at room temperature before serving as a support for metal impregnation. The obtained MSC was dispersed in the ferric chloride solution. The mixture was evaporated 24 h at 50 °C and dried 2 h at 120 °C in a vacuum condition. Finally, the composites were carbonized and reduced 3 h at 850 °C under H_2/N_2 atmosphere in a quartz tube, denoted as nZVI–MSC.

Batch experiments

To each experiment, 0.2 g nZVI–MSC was dispersed into 200 mL Cr(VI) solution. The suspension was stirred vigorously for 2 h with a fixed initial pH adjusted by 0.1 M HCl and 0.1 M NaOH. Aliquots of the aqueous solution were withdrawn at certain time intervals and then analyzed after being filtered through a 0.45 μm membrane filter. The experiment results take the average of three times data. The impacts of initial pH on the removal efficiency of Cr(VI) on nZVI–MSC were tested from 5.0 to 9.0. The initial concentration of Cr(VI) was also studied during 10–80 mg L^{-1}.

Characterization and analysis methods

The microstructure and morphology of prepared mesoporous materials were analyzed with X-ray diffractometer (Bruker, Germany), N_2 adsorption instrument (Quantachrome Autosorb-1, USA) and transmission electron microscopy (TEM) (FEI Tecnai G20 instrument, Czech). The determination of total Cr was tested by a WFX-110 atomic absorption spectrometer (Beijing Rayleigh Analytical Instrument Co., China) using air–acetylene flame. The concentration of Cr(VI) was measured at 540 nm using a UV–Vis spectrophotometer (PE Lambda 35, USA) by the diphenylcarbazide method.

Results and discussion

Physicochemical properties of MSC and nZVI–MSC

Figure 1a shows the small-angle XRD patterns of MSC and nZVI–MSC. MSC exhibits three well-resolved peaks at (100), (110) and (200) similar to the *P6mm* hexagonal symmetry of the SBA-15 (Zhao et al. 1998), which confirmed it with ordered hexagonal structures. For nZVI–MSC, the intensity of the diffraction peaks was not apparently decreased after introduction of the Fe particles, indicating that the ordered mesostructure of MSC has been still retained. Figure 1b shows the wide-angle XRD patterns of MSC and nZVI–MSC. In addition to the diffraction peaks from carbon, a weak and wide diffraction peak at 44.5° corresponding to the formation of zero-valent iron (JCPDS No. 06-0696) could be observed (Saad et al. 2010), which may be attributed to nZVI particles embedded into the walls of the MSC with small size and poor crystallization.

The main pore structure properties of MSC and nZVI–MSC were measured by N_2 adsorption–desorption instrument. Both of them display irreversibly type IV isotherm with a H1 hysteresis loop and a sharp increase in the adsorbed amount of N_2 at relative pressure, $P/P_0 = 0.6$–0.8, characteristic of highly ordered mesoporous materials (Fig. 2). The BET surface area and pore volume of nZVI–MSC are only marginally reduced from those of MSC while the pore diameter stays unchanged (Table 1). This reveals that the uniform mesoporous nature of the material is preserved and no pore-blocking occurred upon the incorporation of Fe. Therefore, nZVI–MSC will exhibit great potential for removal Cr(VI) because of the high surface area and exposed Fe active sites.

TEM analysis was performed to investigate the morphology and the effect of the incorporation of Fe particles on the supports. Figure 3 shows the TEM images of MSC and nZVI–MSC. MSC exhibits well-ordered channels characteristic of 2D hexagonal (*P6mm*) mesostructure with clear and dark lines corresponding to the pores and walls. After introducing the iron species, the structure of nZVI–MSC is still preserved with partially collapse even though the

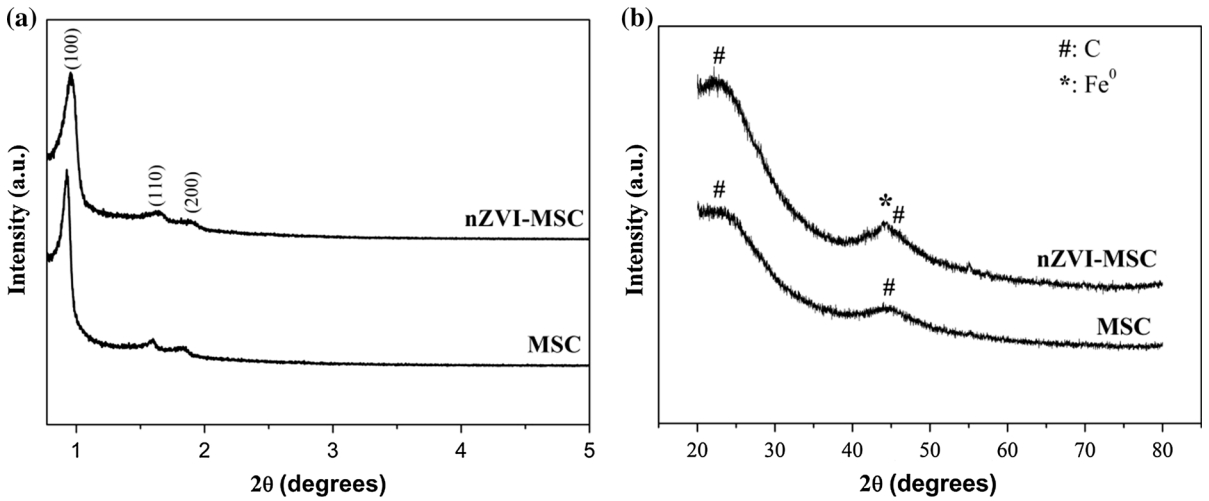

Fig. 1 Small-angle (**a**) and wide-angle (**b**) XRD patterns of MSC and nZVI–MSC

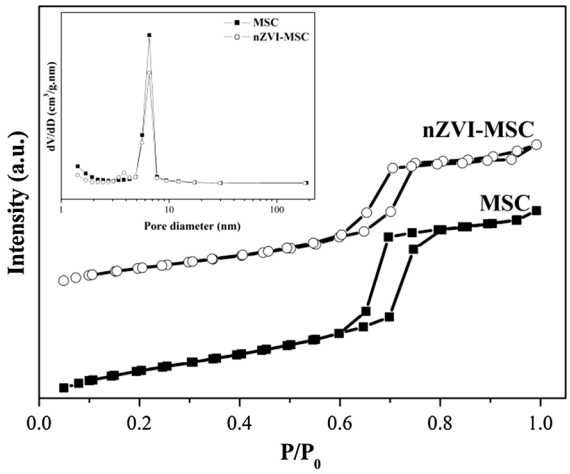

Fig. 2 N_2 adsorption–desorption isotherms curves of MSC and nZVI–MSC (*inset* corresponding pore size distribution curves)

thermal carbonization process was conducted at high temperature (850 °C) (Xiong et al. 2010). Most Fe particles are embedded on the walls and uniformly dispersed on the support within the range of 10 nm, probably due to that the partially carbonized sucrose under high-temperature pyrolysis conditions have abundant oxygen functional groups serving as anchoring sites for iron. Such carbon as an assistant reducing agent under H_2/N_2 atmosphere can react with the anchored iron to form Fe particles embedded on the walls of MSC. The formed nZVI–MSC has a remarkable stability against sintering after the reaction (Fig. 3c). This result is similar to the previous study on the highly dispersed silver nanoparticles supported over the silica via a situ autoreduction route. They found that Ag nanoparticles confined within the mesoporous silica are very stable upon heat treatment and concluded that the high thermal stability of Ag nanoparticles inside the channels of silica can only be attributed to the confinement of ordered mesoporous structures (Sun et al. 2006). The phenomenon of aggregation and arbitrary growth of Fe particles could thus be well constrained by the MSC walls.

Cr(VI) removal efficiencies on MSC, nZVI/AC and nZVI–MSC

Figure 4 shows Cr(VI) removal efficiencies on MSC, nZVI/AC and nZVI–MSC. For pure MSC without nZVI, low removal efficiency with 14 % is from its physical adsorption of porous structure. When nZVI particles are incorporated on the MSC as a remover, the removal efficiency is found to significantly increase to

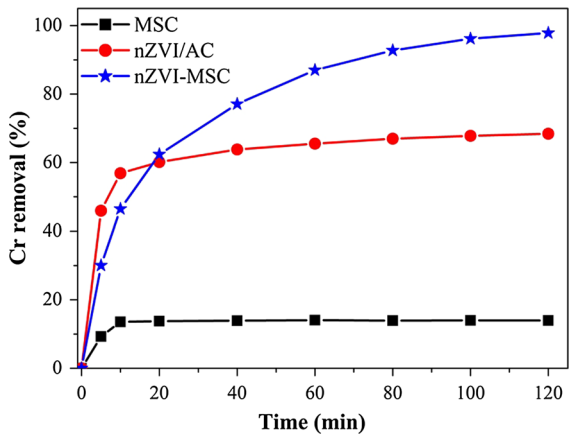

Fig. 4 Comparison of Cr(VI) removal on MSC, nZVI/AC and nZVI–MSC; pH: 7.0; initial Cr(VI) concentration: 20 mg L^{-1}

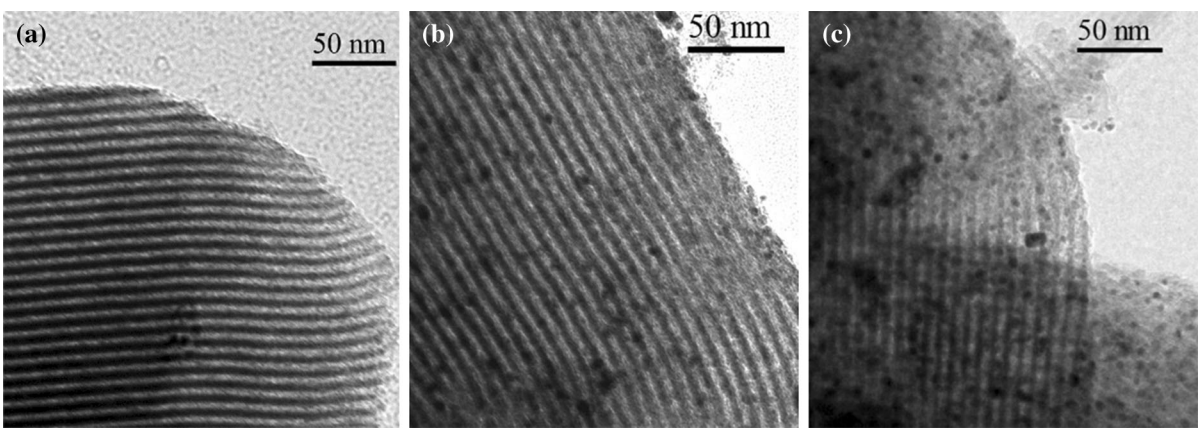

Fig. 3 TEM images of **a** MSC; **b** nZVI–MSC; and **c** spent nZVI–MSC

97 % within 2-h reaction. Such excellent efficiency depended mainly on the adsorption and reduction process by nZVI–MSC with high surface area and unique structure of Fe embedded on the walls. Although nZVI/AC has similar surface area to nZVI–MSC, its removal efficiency is much lower than nZVI–MSC. For nZVI/AC, the Fe particles are supported on the surface of AC, easily forming oxide film during the exposed air and water conditions, resulting in a decrease in reaction rate. In addition, the aggregation and dissolution of the nZVI particles also affect the removal efficiency due to the weak interactions of the nZVI particles and AC. In contrast, for nZVI–MSC, the Cr(VI) in aqueous solution was impregnated into the mesoporous of the MSC due to the effect of capillaries on the physical properties of water. The existence of Fe embedded structure may prolong time for Fe particles to contact with Cr(VI), but this feature create certain micro-electrode on the interface of nZVI and MSC because of the electron transfer, which prevented the formation of metal oxide on the surface and provided fresh nZVI surface for Cr(VI) removal. The impregnated Cr(VI) was absorbed on the incorporated nZVI particles and directly reduced, in which Fe donated electrons to reduce the Cr(VI) to Cr(III). As the reaction went on, the gradient in Cr(VI) concentrations inside and outside the pores was augmented significantly, inducing the Cr(VI) to be continuously pushed into the mesoporous. Therefore, nZVI–MSC exhibits excellent performance for Cr(VI) removal as the reaction went on.

Optimization of pH on Cr(VI) removal efficiency

Solution pH plays an important role with respect to the adsorption of Cr(VI) on the remover. It has been widely reported that pH could change the existing form of Cr(VI). Between pH 2–6, Cr(VI) exists in the form of $HCrO_4^-$; pH 6–7.5, CrO_4^{2-} and $Cr_2O_7^{2-}$; and pH > 7.5, CrO_4^{2-} is the only chromate in aqueous solution (Lv et al. 2011). It can be seen that all of these Cr are negative. So the effect of pH on the Cr(VI) removal efficiency was investigated at 5.0, 7.0 and 9.0, respectively. Figure 5 shows that the removal efficiency decreased from 99.6 to 91.1 % with the increase in the solution pH. Reduction kinetics of Cr(VI) on the nZVI–MSC can be described by a pseudo first-order model, $\ln(C_t/C_0) = -k_{obs}t$, where k_{obs} is the observed pseudo first-order rate constant (min^{-1}), t is the reaction time (min), C_t is the instantaneous concentration of Cr(VI), C_0 is the initial concentration of Cr(VI) (Ponder et al. 2000; Rangsivek and Jekel 2005). As presented in Fig. 5 (inset), k_{obs} decreased from 0.1104 to 0.0182 min^{-1} when the solution pH increased from 5.0 to 9.0. These results suggest that the lower solution pH is favor of Cr(VI) removal by the nZVI–MSC. According to the mechanism of Cr(VI) removal on the nZVI (Sun et al. 2014; Chen et al. 2015), the adsorption process that is induced by electrostatic, hydrophobic and hydrogen bond interactions mainly depends on the solution pH. Furthermore, pH affects the surface charge of nZVI–MSC. When pH is under the pH of zero point charge (pH_{zpc}), the positive surface charge makes it easier to adsorb the negative Cr(VI). On the contrary, it will produce electrostatic repulsion, resulting in low removal efficiency (Pradhan et al. 1999; Das et al. 2002; Mor et al. 2007). During the reduction process, the effect of pH can be clearly expressed by the following Eqs. (1–4). A lot of H^+ is consumed all along the reaction. This explained why an acidic environment is preferred by the Cr(VI) removal in aqueous solution. In addition, the hydrophobic and hydrogen bond interactions increased as pH decreased, which further enhanced the removal efficiency of Cr(VI) (Kun and Xing 2009).

$$2HCrO_4^- + 3Fe + 14H^+ \rightarrow 3Fe^{2+} + 2Cr^{3+} + 8H_2O \quad (1)$$

$$2CrO_4^{2-} + 3Fe + 16H^+ \rightarrow 3Fe^{2+} + 2Cr^{3+} + 8H_2O \quad (2)$$

Table 1 Surface and porous characteristics of MSC, nZVI–MSC and nZVI–AC

Samples	Surface area (m^2/g)	Average pore diameter (nm)	Total pore volume (cm^3/g)
MSC	515	6.5	1.036
nZVI–MSC	437	6.5	0.716
nZVI–AC	421	2.5	0.273

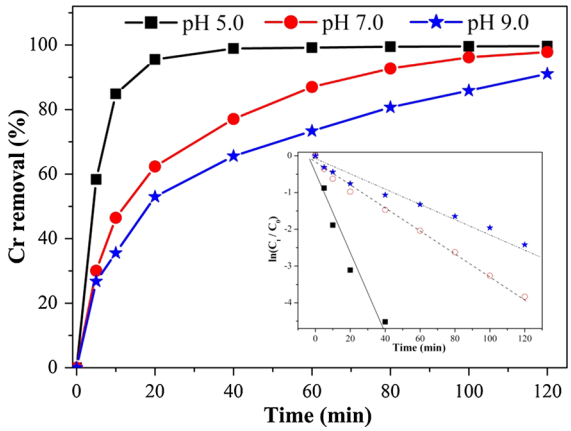

Fig. 5 Effect of pH on Cr(VI) removal (*inset* modeling of the kinetics by fitting to the pseudo first-order reaction); initial Cr(VI) concentration: 20 mg L^{-1}

$$HCrO_4^- + 3Fe^{2+} + 7H^+ \rightarrow 3Fe^{3+} + Cr^{3+} + 4H_2O \quad (3)$$

$$2CrO_4^- + 3Fe^{2+} + 8H^+ \rightarrow 3Fe^{3+} + Cr^{3+} + 4H_2O \quad (4)$$

Effect of initial Cr(VI) concentration on the removal efficiency

Figure 6 shows Cr(VI) removal efficiencies on the nZVI–MSC in the different concentration Cr(VI) solution. It can be seen that Cr(VI) was well removed at concentration of 10–60 mg L^{-1}. When the initial Cr(VI) concentration further increased to 80 mg L^{-1}, it began to decrease on the removal efficiency. This suggests that nZVI–MSC has reached saturation at 60 mg L^{-1} Cr(VI) concentration. In this work, we fixed the dosage of nZVI–MSC with 1.0 g L^{-1}, and the adsorption capacity and active sites are certainly constant. When excessive Cr(VI) was added into the solution, limited Fe-MSC cannot remove them well due to lack of enough adsorption capacity and active sites to work with the increase in initial Cr(VI) concentration.

Interference from coexisting anions

As all of Cr(VI) in aqueous solution is negative in valence, some common foreign anions were selected as the coexisting anions to study their effects on the Cr(VI) removal in this work. Figure 7 shows that most of foreign anions did not interface with the Cr(VI) removal, only slow down the removal speed. Some studies (Liu et al. 2009; Lv et al. 2013; Tanboonchuy et al. 2012) reported that the affinity of NO_3^-, HCO_3^- and PO_4^{3-} for iron (oxy)hydroxides is strong through the formation of inner-sphere complexes, which might compete for the same binding sites with dichromate ions and thus retard the removal of Cr(VI). However, adding SO_4^{2-} has obviously negative effect on the removal efficiency with 67 %, which is similar to previous reports (Pillay et al. 2009; Choi and Al-Abed 2010). Such impact may be in two aspects: One is to compete with dichromate ions for the surface area of nZVI–MSC due to the chemical similarity with

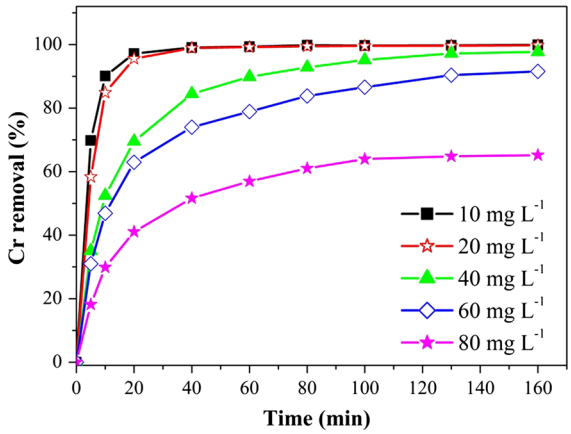

Fig. 6 Effect of initial Cr(VI) concentration on Cr(VI) removal; pH: 5.0

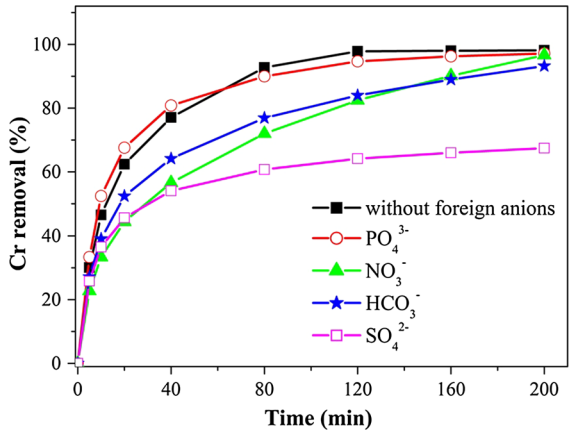

Fig. 7 Effect of foreign anion species for Cr(VI) removal on nZVI–MSC; pH: 7.0; initial Cr(VI) concentration: 20 mg L^{-1}

dichromate ions and the other is the catalyst poisoning of sulfate species (Lowry and Reinhard 2000).

Conclusions

The nZVI–MSC reported here has stable nZVI particles embedded on the walls and retains the ordered pore structures of MSC. Such unique structure is beneficial for enhancing the dispersion of the nZVI particles and providing a large available surface area for the chemical reaction to occur. Furthermore, the intimate contact between nZVI particles and MSC might create certain micro-electrode on the interface, which prevented the formation of metal oxide on the surface and provided fresh Fe surface for Cr(VI) removal. As a result, the nZVI–MSC exhibited excellent performance for Cr(VI) removal. This work may open up a new route toward designing nZVI embedded on the supports with controllable structure for pollutant removal from water bodies.

Acknowledgments This work was financially sponsored by the National Natural Science Foundation of China (Grant No.: 21606028), by the Science and Technology Project from Chongqing Education Commission (KJ1500625, KJZH14210) and by the Scientific Research Foundation of Chongqing Technology and Business University (2016-56-03).

References

Chen D, Yang K, Wang H, Zhou J, Zhang H (2015) Cr(VI) removal by combined redox reactions and adsorption using pectin-stabilized nanoscale zero-valent iron for simulated chromium contaminated water. RSC Adv 5:65068–65073

Choi H, Al-Abed SHR (2010) Effect of reaction environments on the reactivity of PCB (2-chlorobiphenyl) over activated carbon impregnated with palladized iron. J Hazard Mater 179:869–874

Choi H, Al-Abed SR, Agarwa IS, Dionysiou DD (2008) Synthesis of reactive nano-Fe/Pd bimetallic system-impregnated activated carbon for the simultaneous adsorption and dechlorination of PCBs. Chem Mater 203:649–3655

Das DD, Mahapatra R, Pradhan J, Das SN, Thakur RS (2002) Removal of Cr(VI) from aqueous solution using activated cow dung carbon. J Colloids Interface Sci 232:235–240

Jiang WJ, Pelaez M, Dionysiou DD, Entezari MH, Tsoutsou D, O'Shea K (2013) Chromium (VI) removal by maghemite nanoparticles. Chem Eng J 222:527–533

Kun Y, Xing BS (2009) Adsorption of fulvic acid by carbon nanotubes from water. Environ Pollut 157:1095–1100

Liu TZ, Rao PH, Lo IMC (2009) Influences of humic acid, bicarbonate and calcium on Cr(VI) reductive removal by zero-valent iron. Sci Total Environ 407:3407–3414

Lowry GV, Reinhard M (2000) Pd-catalyzed TCE dechlorination in groundwater: solute effects, biological control, and oxidative catalyst regeneration. Environ Sci Technol 34:3217–3223

Lv XS, Xu J, Jiang GM, Xu XH (2011) Removal of chromium (VI) from wastewater by nanoscale zero-valent iron particles supported on multiwalled carbon nanotubes. Chemosphere 85:1204–1209

Lv X, Hu Y, Tang J, Sheng TT, Jiang GM, Xu XH (2013) Effects of co-existing ions and natural organic matter on removal of chromium (VI) from aqueous solution by nanoscale zero valent iron (nZVI)–Fe_3O_4 nanocomposites. Chem Eng J 218:55–64

Miretzky P, Cirelli AF (2010) Cr (VI) and Cr(III) removal from aqueous solution by raw and modified lignocellulosic materials: a review. J Hazard Mater 180:1–19

Mor S, Ravindra K, Bishnoi NR (2007) Adsorption of Cr(VI) from aqueous solution by activated alumina and activated charcoal. Bioresour Technol 98:945–957

Owlad M, Aroua MK, Daud WAW, Baroutian S (2009) Removal of hexavalent chromium-contaminated water and wastewater: a review. Water Air Soil Pollut 200:59–77

Pillay K, Cukrowka EM, Coville NJ (2009) Multi-walled carbon nanotubes as adsorbents for the removal of parts per billion levels of hexavalent chromium from aqueous solution. J Hazard Mater 166:1067–1075

Ponder SM, Darab JG, Mallouk TE (2000) Remediation of Cr(VI) and Pb(II) aqueous solutions using supported nanoscale zero-valent iron. Environ Sci Technol 4:2564–2569

Pradhan J, Das SN, Thakur RS (1999) Adsorption of hexavalent chromium from aqueous solution by using activated red mud. J Colloids Interface Sci 217:137–141

Rangsivek R, Jekel MR (2005) Removal of dissolved metals by zero-valent iron (ZVI): kinetics, equilibria, processes and implications for stormwater runoff treatment. Water Res 39:4153–4163

Saad R, Thiboutot S, Ampleman G, Dashan W, Hawari J (2010) Degradation of trinitroglycerin (TNG) using zero-valent iron nanoparticles/nanosilica SBA-15 composite (NZVIs/SBA-15). Chemosphere 81:853–858

Selvi K, Pattabhi S, Kadirvelu K (2001) Removal of Cr(VI) from aqueous solution by adsorption onto activated carbon. Bioresour Technol 80:87–89

Sheng G, Hu J, Li H, Li JX, Huang YY (2016) Enhanced sequestration of Cr(VI) by nanoscale zero-valent iron supported on layered double hydroxide by batch and XAFS study. Chemosphere 68:1861–1866

Shipley HJ, Engates KE, Guettner AM (2011) Study of iron oxide nanoparticles in soil for remediation of arsenic. J Nanopart Res 13:2387–2397

Singh R, Misra V, Singh RP (2011) Synthesis, characterization and role of zero-valent iron nanoparticle in removal of hexavalent chromium from chromium-spiked soil. J Nanopart Res 13:4063–4073

Sun JM, Ma D, Zhang H, Liu XM, Han XW, Bao XH, Weinberg G, Pfander N, Su DS (2006) Toward monodispersed silver

nanoparticles with unusual thermal stability. J Am Chem Soc 128(49):15756–15764

Sun X, Yan YB, Li JS, Han WQ, Wang LJ (2014) SBA-15-incorporated nanoscale zero-valent iron particles for chromium (VI) removal from groundwater: mechanism, effect of pH, humic acid and sustained reactivity. J Hazard Mater 266:26–33

Tanboonchuy V, Grisdanurak N, Liao CH (2012) Background species effect on aqueous arsenic removal by nano zero-valent iron using fractional factorial design. J Hazard Mater 205–206:40–46

Wang QL, Snyder S, Kim J, Choi H (2009) Aqueous ethanol modified nanoscale zero valent iron in bromate reduction, synthesis, characterization, and reactivity. Environ Sci Technol 43:3292–3299

Wang G, Chang Q, Han XT, Zhang MY (2013) Removal of Cr(VI) from aqueous solution by flocculant with the capacity of reduction and chelation. J Hazard Mater 248–249:115–121

Wu YW, Zhang J, Liu JF, Chen L, Deng ZL, Han MX, Wei XS, Yu AM, Zhang HL (2012) Fe_3O_4@ZrO_2 nanoparticles magnetic solid phase extraction coupled with flame atomic absorption spectrometry for chromium(III) speciation in environmental and biological samples. Appl Surf Sci 258:6772–6776

Xiong K, Li JL, Liew KY, Zhan XD (2010) Preparation and characterization of stable Ru nanoparticles embedded on the ordered mesoporous carbon material for applications in Fischer–Tropsch synthesis. Appl Catal A Gen 389:173–178

Zhang YY, Jiang H, Zhang Y, Xie JF (2013) The dispersity-dependent interaction between montmorillonite supported nZVI and Cr(VI) in aqueous solution. Chem Eng J 229:412–419

Zhao DY, Huo QS, Feng JL, Chmelka BF, Stucky GD (1998) Nonionic triblock and star diblock copolymer and oligomeric surfactant syntheses of highly ordered, hydrothermally stable, mesoporous silica structures. J Am Chem Soc 120:6024–6036

Zheng Y, Yang JX, Zheng WL, Wang X, Xiang C, Tang L, Zhang W, Chen SY, Wang HP (2013) Synthesis of flexible magnetic nanohybrid based on bacterial cellulose under ultrasonic irradiation. Mater Sci Eng C 33:2407–2412

Zhitkovich A (2005) Importance of chromium-DNA adducts in mutagenicity and toxicity of chromium (VI). Chem Res Toxicol 18:3–11